

Article

Influence of the Anodizing Time on the Microstructure and Immersion Stability of Tartaric-Sulfuric Acid Anodized Aluminum Alloys

Florian Raffin ¹, Jacques Echouard ² and Polina Volovitch ^{1,3,*}

¹ Chimie ParisTech-CNRS, Institut de Recherche de Chimie Paris (IRCP), PSL University, 11 rue Pierre et Marie Curie, 75005 Paris, France; florian.raffin@chimieparistech.psl.eu

² Safran Landing Systems, 7 Rue Général Valérie André, 78140 Vélizy-Villacoublay, France

³ Institut Photovoltaïque d'Île-de-France (IPVF), UMR 9006, CNRS, Ecole Polytechnique, IP Paris, Chimie ParisTech, PSL University, 91120 Palaiseau, France

* Correspondence: polina.volovitch@chimieparistech.psl.eu

Abstract: Tartaric-sulfuric acid anodizing (TSA) has been selected by the aerospace industry to replace Cr(VI)-based anodizing treatments of aluminum alloys. Modification of the bath composition can result in the necessity to revise the process conditions, including the time necessary to obtain the desired properties of the anodized layer. This study focuses on the microstructure and immersion stability of the pilot scale anodized AA2024 aluminum alloy, with anodizing times of 25 min and 45 min. The layer structure was characterized by scanning electron microscopy (SEM) and glow discharge optical emission spectrometry (GD-OES). The electrochemical impedance spectroscopy (EIS) was used to evaluate the corrosion resistance and immersion stability of the samples in 0.01 M NaCl solution. The density of pores formed in the 45 min anodized samples was higher which correlated with higher impedance modulus at equivalent immersion time and higher thickness of the oxide layer. Contact angle measurements demonstrated better wettability of the 45 min anodized sample. The results suggest that 45 min anodizing offers higher corrosion resistance and better initial adhesion with subsequent post-treatment such as sealing or painting.

Keywords: TSA anodizing; aluminum alloy; electrochemical impedance spectroscopy; corrosion protection



Citation: Raffin, F.; Echouard, J.; Volovitch, P. Influence of the Anodizing Time on the Microstructure and Immersion Stability of Tartaric-Sulfuric Acid Anodized Aluminum Alloys. *Metals* **2023**, *13*, 993. <https://doi.org/10.3390/met13050993>

Academic Editors: Guosong Wu, Jiapeng Sun and Hao Wu

Received: 12 April 2023

Revised: 16 May 2023

Accepted: 17 May 2023

Published: 20 May 2023



Copyright: © 2023 by the authors. Licensee MDPI, Basel, Switzerland. This article is an open access article distributed under the terms and conditions of the Creative Commons Attribution (CC BY) license (<https://creativecommons.org/licenses/by/4.0/>).

1. Introduction

In the aerospace industry, aluminum alloys of 2xxx (containing mainly Cu and Mg) and 7xxx (containing mainly Zn, Mg and Cu) series are the first-choice materials especially because of their weight to strength ratio. The corrosion resistance needs however to be enhanced to satisfy the standards of the aerospace application [1,2]. This is usually achieved by application of specific coatings, including polymer coatings (paints) and surface treatments. For both painted and unpainted applications, one of the most common surface treatments for aluminum alloys is anodizing, forming a low porous aluminum oxide layer thanks to the electrochemical oxidation in acidic solution [3]. Hard anodizing is used in some applications (hydraulics for example) and results in an oxide layer thickness of several tenths of a micron. However, for applications such as automotive, aerospace or as a pre-treatment for paint, thinner oxide layers are necessary because of specific designs and the need for optimal mechanical surface properties [3]. Historically, among widely used sulfuric acid anodizing (SAA), some processes were based on an electrolyte containing chromic acid, so hexavalent chromium (Cr(VI)). This compound belongs however to the list of carcinogenic, mutagenic and reprotoxic (CMRs) substances. According to the European Union regulation monitoring the use of such toxic compounds (Registration, Evaluation and Authorization of Chemicals “REACH” regulation), including chromate species, should be

banned by 2024 in the aerospace industry. As a consequence, several Cr(VI)-free alternatives have been proposed. Among them, boric-sulfuric acid (BSA), sulfuric acid anodizing (SAA) or tartaric-sulfuric acid (TSA) were proposed. Several studies [4–12] display anodizing in a TSA bath as a very promising solution for Chromium Acid Anodizing (CAA) substitution, and it is already operative in some industrial plants. The structure of the oxide layer formed during anodizing, from the thickness to the pore diameter for example, depends on numerous parameters. The influence of these parameters (voltage, bath temperature, or nature of the electrolyte) on the anodic layer properties is well documented [5,12–19]. For example, increasing the temperature of the bath increases the thickness of the oxide layer but can also impact the pore morphology [14]. Schneider et al. [16] reported that the ejection of Al^{3+} ions in the anodizing bath during dissolution of the oxide changes the bath concentrations and its efficiency, leading to morphological modification of the porous microstructure. However, few studies are focused on the effect of the anodizing time [20,21] in pilot plants. It is known that the oxide layer growth is faster at the beginning of the anodizing step because of the decreasing conductivity of the formed anodic layer [21]. Moreover, the growth of the layer is not infinite as the competition between the oxide dissolution and its growth reaches an equilibrium. It was shown that longer anodizing led to thicker oxide layers [20,21]. García-Rubio demonstrated that a short anodizing time (10 min) resulted in poor corrosion resistance compared to a longer time (20 and 30 min) [21]. Mubarak et al. [20] came to similar conclusion (increasing thickness with increased anodizing time) but going up to an anodizing time of 60 min. However, such a long anodizing time may not be suitable for industrial conditions because the prices increase with the process time. A compromise between the process price and the coating efficiency is necessary. Thus, the novelty of this work resides in the more detailed understanding of the impact of anodizing time on the detailed microstructure and chemistry of the formed layer and its anticorrosion properties, which is an important step to achieve this compromise. In particular, it verifies if there is an improvement of corrosion protection with longer anodizing time and if it should be attributed to the increased thickness or porosity modification in the porous layer or improvement of the barrier layer.

The present work aims toward a better understanding of the effect of increasing anodizing time on the oxide layer microstructure and its immersion stability on the example of 2024 and 7075 Al alloys anodized in a TSA bath in pilot conditions. The morphology of the oxide layer was characterized by scanning electron microscopy (SEM); the in-depth chemical distribution of the elements was evaluated with glow discharge–optical emission spectroscopy (GD-OES), and the electrochemical stability of the immersed samples was assessed by electrochemical impedance spectroscopy (EIS).

2. Materials and Methods

2.1. Materials

Specimens from the AA2024–T3, AA7075–T6 and AA7175–T6 alloys with a thickness of 0.5 cm were produced by rolling and cutting them into samples of $10 \times 12 \text{ cm}^2$. Nominal chemical composition of the alloys is given in Table 1. Anodizing was made in pilot conditions (200 L bath) on the plates previously degreased in a 10% vol. alkali-based bath (silicate-free, $\text{pH} = 9$) for 10 min at $45 \text{ }^\circ\text{C}$. Rinsing with deionized water was applied between each step. Etching was then performed during 10 min at $50 \text{ }^\circ\text{C}$ in a mix of 42% vol. acid-based solution (sulfuric and nitric acid) and 10% vol. ferric sulfate-based solution (bath $\text{pH} < 1$). The specimens were then anodized in a tartaric/sulfuric acid (TSA) bath (80 g/L of $\text{C}_4\text{H}_4\text{O}_6$ and 40 g/L of H_2SO_4) at $37 \text{ }^\circ\text{C}$ for either 25 min or for 45 min. The applied voltage was 14 V, a value reached after 5 min of voltage ramp, included in the time specified above. A power supply device from Micronics Systems (Villette d’Anthon, France) was used.

Table 1. Nominal chemical composition of alloys (wt.%). Bal.—balance to arrive to 100%.

Al Alloy	Si	Fe	Cu	Mn	Mg	Cr	Zn	Ti	Others	Al
AA2024-T3	0.5	0.5	3.8–4.9	0.3–0.9	1.2–1.8	0.1	0.25	0.15	0.15	Bal.
AA7075-T6	0.4	0.5	1.2–2.0	0.3	2.1–2.9	0.18–0.28	5.1–6.1	0.2	0.15	Bal.
AA7175-T6	0.15	0.2	1.2–2.2	0.1	2.1–2.9	0.18–0.28	5.1–6.1	0.1	0.15	Bal.

For the control of the obtained layers, thickness of the oxide was verified with Foucault current measurement. A thicker oxide layer was obtained for 45 min anodizing (5 to 8 μm thick compared to 4 to 7 μm thick for 25 min anodizing). The observations by SEM gave similar values.

The surface roughness was assessed with a VHX-5000 optical 3D microscope (Keyence, Bois-Colombes, France) and image treatment with Gwyddion software.(version 2.62, Gwyddion) There were no meaningful differences between the samples, and the obtained parameters were Roughness Average (Ra) which was $2.4 \pm 0.2 \mu\text{m}$ and Root Mean Square (RMS) which was $2.8 \pm 0.2 \mu\text{m}$.

2.2. Scanning Electron Microscope (SEM) and Porosity Measurement

The surface morphology of the sample after anodization was observed with a LEO-1530 field emission gun scanning electron microscope (FEG-SEM) (Carl Zeiss SAS, Rueil Malmaison, France). To limit the charging effect, the operating tension was 1 keV, and the working distance was 4 mm. No carbon was deposited on the surface to avoid pollution of the porous microstructure. ImageJ software (version 1.53e, National Institutes of Health, USA) was used to calculate porosity parameters. The surface images were recorded at magnification allowing the distinguishing of the pores with a diameter of several nm, as illustrated on the example of 45 min anodized 2024 alloy in Figure 1a. Several representative high resolution SEM images coming from 2 different locations with a cumulated analyzed area of surface of about $1.5 \mu\text{m}^2$ were analyzed for each of two samples. Images were treated in the 8-bit format. The equivalent pixel distance for one nm was 0.92 pixels. After image scale calibration, a threshold operation was applied to each image to highlight the pores and obtain porosity parameters, as illustrated in Figure 1b. Only pores with a size above 20 nm^2 were considered, and those on the edges of the image were excluded. The average area of the pore (in nm^2) was obtained and converted to nm in an assumption of a circular section of the pore to obtain the average pore diameter. The porosity was calculated as the area fraction of black pixel in the threshold-treated image.

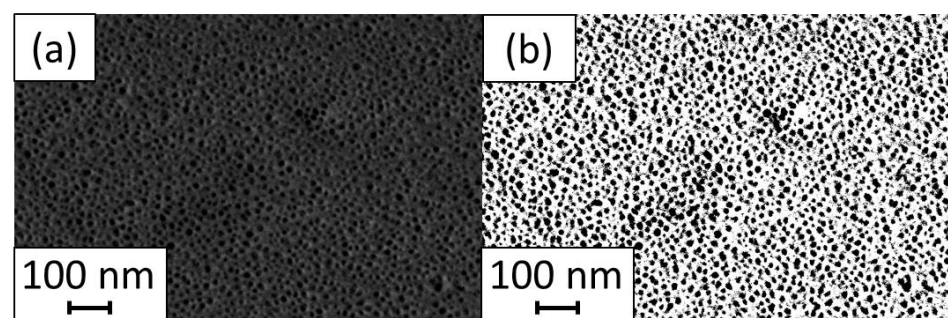


Figure 1. Example of SEM in-lens secondary electron image showing surface morphology of 2024 alloy after 45 min anodizing before (a) and after (b) threshold operation in ImageJ software (version 1.53e, National Institute of the Health, MD, USA).

2.3. Glow Discharge–Optical Emission Spectroscopy (GD-OES)

Depth profiles were obtained with a GD-Profilier 2TM (Horiba France SAS, Palaiseau, France). Homogeneous sputtering was obtained with a 4 mm-diameter anode and the following plasma conditions: Ar plasma, a pressure of 900 Pa and a power of 35 W. The

emission lines of 48 species were recorded simultaneously on the polychromator, but only the relevant elements are discussed in this article. The lines of interest are oxygen (130 nm), nitrogen (149 nm), sulfur (181 nm), aluminum (396 nm), copper (325 nm) and magnesium (285 nm). In order to represent the in-depth variation of the relative intensity of the displayed elements, all the signals were normalized by the total light emitted by the plasma (I_i).

2.4. Electrochemical Impedance Spectroscopy (EIS)

A Gamry 3000 potentiostat (Gamry Instruments, Warminster, PA, USA) equipped with the Gamry Framework™ (version 7.07, Gamry Instruments, Warminster, PA, USA), and Gamry Echem Analyst™ (version 7.07, Gamry Instruments, Warminster, PA, USA) software was used to perform electrochemical impedance spectroscopy (EIS). A three-electrode set-up was employed, consisting of a graphite rod (6.6 mm diameter) as a counter electrode (CE), a silver/silver-chloride (Ag/AgCl) as a reference electrode (RE) and the sample as a working electrode (WE). The active surface of 12.56 cm² was delimited by an O-ring. Samples were immersed in 40 mL of 0.01 M NaCl, without stirring for a maximum duration of 75 h. After 90 min of open circuit potential (OCP) stabilization, EIS was measured every 2 h during immersion. The impedance measurements were performed at the OCP with a 15 mV root mean square (rms) amplitude in the frequency range from 100 kHz to 0.05 Hz and 7 points per frequency decade.

2.5. Contact Angle (CA) Measurements

Contact angle was measured in order to compare the wettability of the surface after anodizing and assess the possible change on the initial adhesion of the layer with post-treatments (organic coating for example). Before the analysis, the surface of the samples was rinsed with ethanol and dried with compressed air. Contact angle measurements were performed on a OCA 15 Pro device (DataPhysics Instruments, Filderstadt, Germany), using the sessile drop method to assess the wettability of the samples. The deposited liquid was ultrapure water generated by a water purification system Direct-Q® 3 UV (Merck Chimie SAS, Fontenay-sous-Bois, France). A drop of 12 µL was deposited at a rate of 2 µL/s through an Injekt®-F syringe (B. Braun, Saint-Cloud, France) of 1 mL mounted with a needle (diameter of 0.51 mm). Measurements were made with the Dataphysics SCA 20 software (version 1.0, DataPhysics Instruments, Filderstadt, Germany). To obtain reproducible values and estimate the surface disparities of the sample, the contact angle value, displayed in the next sections is an average of 10 measurements spread on the whole surface.

3. Results

3.1. Microstructure of the Anodized Surface

Firstly, the microstructure of the oxide layer was observed by SEM. Figure 2a,b displays the surface microstructures of the 2024 anodized for 25 min at different scales. The overall morphology shows roughness, and the pores formed by the anodizing process can be observed in Figure 2b. Figure 2c,d shows the surface of the 2024 anodized for 45 min.

The overall surface seems to have more surface inhomogeneities for the oxide layer anodized for 25 min than for that anodized for 45 min. Red arrows point out these differences, as the surface appears smooth in some areas (red arrow in Figure 2c) while it can also present a cauliflower morphology (red arrow in Figure 2a). Several defects are visible on the 25 min anodized surface, which are generally attributed to the preferential dissolution of the intermetallic particles enriched in copper during the anodizing step in the TSA bath [22–26]. The average pore diameter estimated by the image analysis demonstrated close value for 25 min and for the 45 min anodized surface around 14 nm. No standard deviation for the pore diameter value is presented as the data distribution was large. This is represented by the histograms in Figure 3. More details about pores size can be found in Supplementary Information, Figure S1. The difference between two types of the samples is even more pronounced in the area fraction occupied by pores (Table 2). The image analysis gives a porosity of 30.0% for the 45 min-anodized and 15.0% for the

25 min-anodized samples. As the pore diameter is close for the two samples, the higher porosity means that the pore walls are thinner for the 45 min anodized sample. Compared to the literature, the morphology of the pores of 45 min TSA anodized sample is closer to CAA aluminum alloys than the 25 min TSA anodized morphology [27].

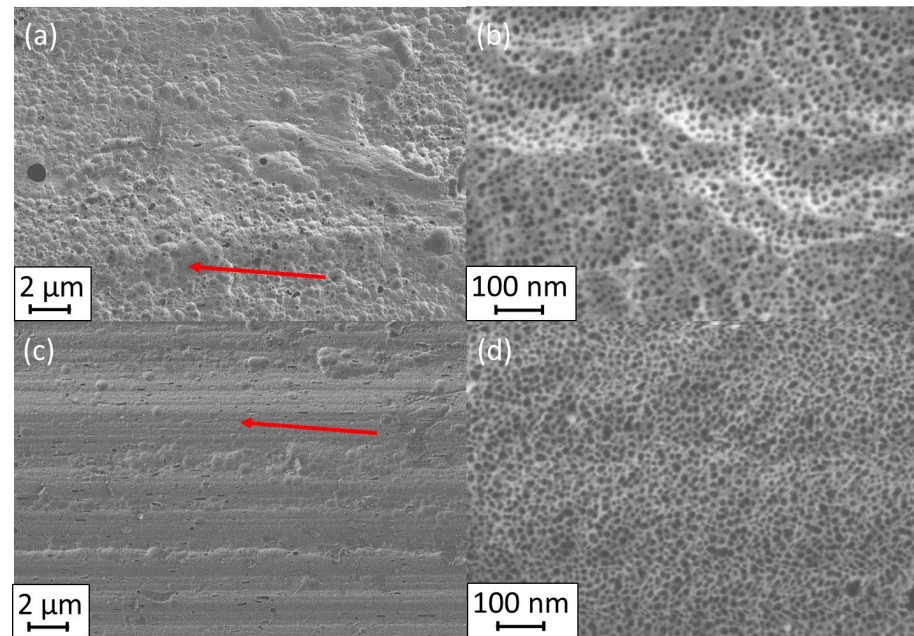


Figure 2. SEM surface morphology of 2024 after anodizing in TSA for 25 min (a,b) and 45 min (c,d). Red arrows point out different surface morphologies.

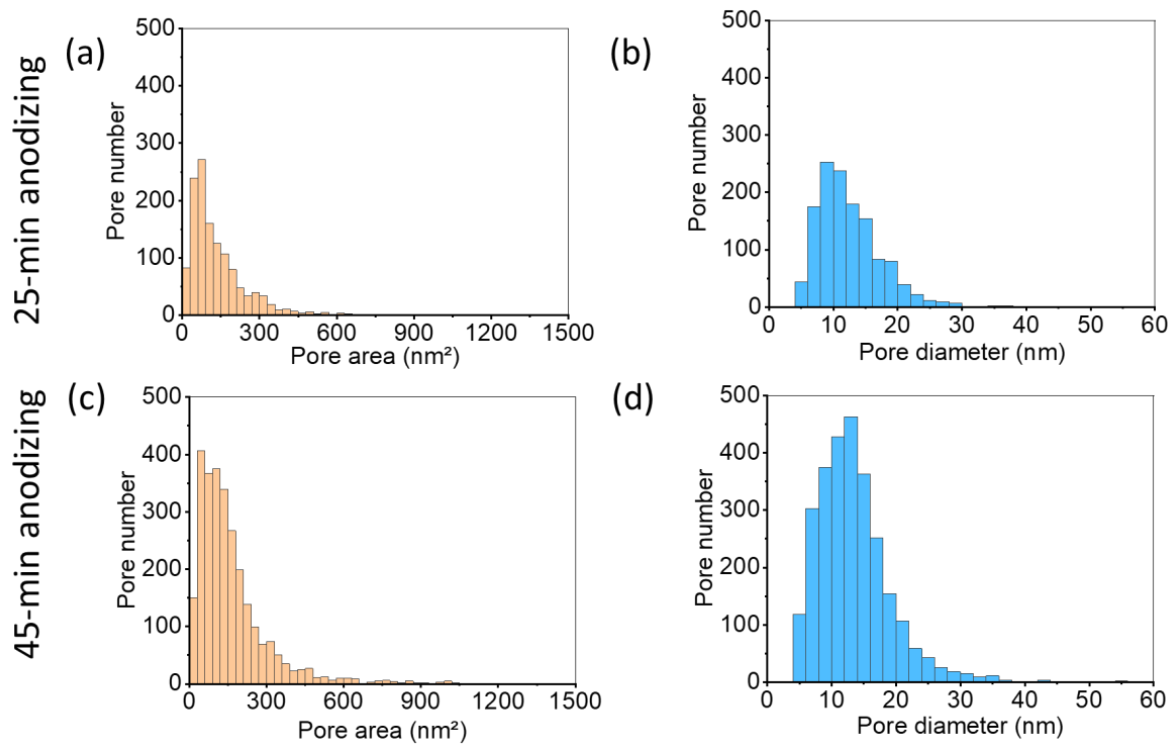


Figure 3. Data distribution of measured pore area and pore diameter calculated in approximation of a circular section for 2024 after anodizing in TSA for 25 min (a,b) and 45 min (c,d).

Table 2. Pore size parameters obtained from image analysis.

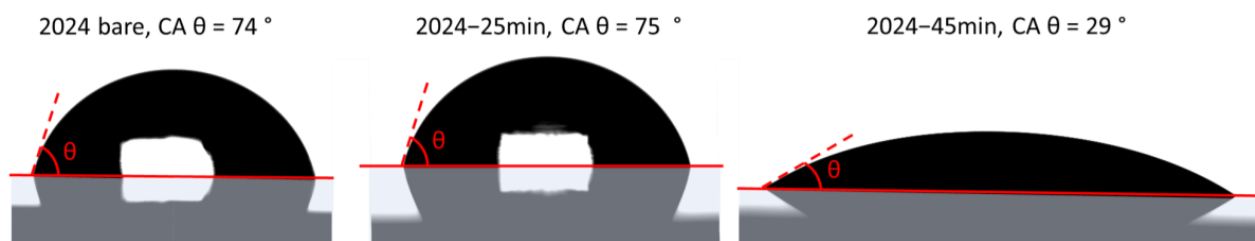
Sample	Average Pore Size (nm ²)	Area (%)	Average Pore Diameter (nm)	Pores Number
2024 after 25 min anodizing	140.9	15.0 ± 1.1	13.3	1303
2024 after 45 min anodizing	167.7	30.0 ± 0.3	14.6	2753

3.2. Wettability of the Oxide Layer

The impact of the anodized surface porosity on the wettability was estimated through contact angle (CA) measurements with ultrapure water. The results are shown in Table 3. Several surfaces are compared: non-anodized 2XXX and 7XXX series alloys (bare alloys), the same alloys anodized with the 25 min and 45 min cycle. For the 7XXX series, 7175 was used in some measurements instead of 7075 because of an insufficient number of samples and the extremely close composition of the two alloys (see Table 1). Typical water contact angle micrographs for the 2024 series are displayed in Figure 4. The wettability of bare alloys is low which is reflected by high values of the contact angle. Anodizing seems to decrease the contact angle for both series of aluminum alloy, suggesting a better wettability of the anodized surface. Wettability seems to increase with anodizing duration. The values of the tested 45 min anodizing sample are in the scope of values of water contact angle for CAA 2024 found in the literature (27.0 ± 2.8 for 45 min anodizing vs. 16.5 ± 3.0 for CAA 2024) [28].

Table 3. Contact angle with ultrapure water on 2024 and 7075/7175 samples.

Sample	No Anodizing		25 min Anodizing		45 min Anodizing	
	2024–bare	7075–bare	2024–25 min	7075–25 min	2024–45 min	7175–45 min
Contact angle (°)	74.5 ± 4.4	80.9 ± 5.4	75.8 ± 8.3	62.5 ± 8.4	27.0 ± 2.8	39.0 ± 1.8

**Figure 4.** Typical Contact angle (CA) θ is shown on micrographs for 2024 bare alloy, 2024–25 min and 2024–45 min. The horizontal red line delimits the surface of the sample. The white shaded area below each horizontal red line is due to reflection.

3.3. Chemical Composition and In-Depth Element Distribution

To verify the composition of the anodic film and the in-depth element distribution, GD-OES measurements were performed. Typical elemental depth profiles of the 25 and 45 min anodized samples are presented in Figure 5.

For both samples, three distinct parts can be defined on the profiles, which can be tracked by the signals of specific elements. The anodized layer (part I) is evidenced by the O and S plateau. In the substrate alloy (part III), Al and alloying elements (Cu, Mg) are maximized while O and S signals are at the level of their background. The transition zone between the oxide layer and the substrate alloy (part II) is relatively long reflecting a relatively rough interface between the layers. The Al plateau signal is low in the oxidized layer (part I), and it increases at the interface to reach a high intensity plateau when the substrate erosion occurs. Signals from the alloying elements are quasi zero in the oxide zone and follow a similar trend as Al in the interface and the substrate, confirming the presence of magnesium or copper in the bulk alloy.

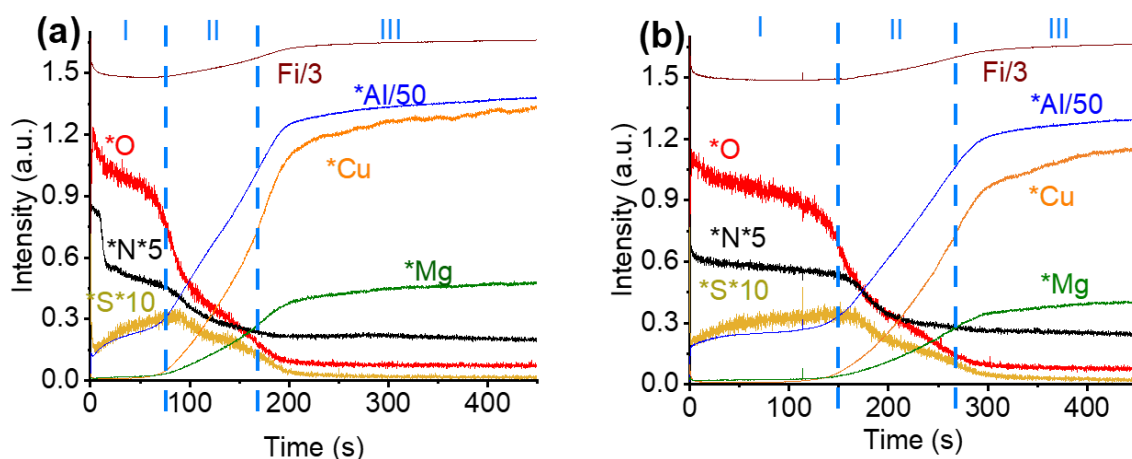


Figure 5. GD-OES elemental depth profile of 2024 after 25 min anodizing (a) and after 45 min anodizing (b). Zone I is the oxide layer; zone II is the transition through the bulk, and zone III is the substrate. Fi is the total light emitted during erosion. The * symbol means that displayed signals were normalized by the Fi signal, more details are available in Section 2.3.

For both samples, a high S intensity is detected homogeneously throughout the anodized layer (part I) which is coherent with previous studies [29,30], confirming sulfates incorporation in the coating.

The nitrogen signal is interesting because N_2 gas is the major component of the air which can be adsorbed inside the pores. Thus, following its signal is interesting to evaluate the porosity of the porous oxide layer, as long as there is no N in the material composition at first. Except for the first seconds of erosion, which can be related to a possible surface contamination, the N signal intensity was higher for the 45 min anodized sample as illustrated on the example of the profiles in Figure 5. This result is coherent with the previously described SEM observations of higher porosity for 45 min anodized samples than for that which was 25 min anodized.

The main difference between the two depth profiles presented in Figure 5a,b resides in the sputtering time necessary to reach the bulk alloy erosion (part III). In the case of the 25 min anodized sample, this time is approximately 170 s (Figure 5a). The same value is much higher for the longer anodizing time sample, as it reaches almost 270 s (Figure 5b). This difference proves that it takes more time to reach the substrate for the longer anodizing cycle. This can be either due to the slower erosion rate or to a thicker oxide layer. The fact that the total light emitted of Fi has an identical shape and intensity for both samples indicates that the erosion rate should be similar. This allows the consideration of the erosion time as a measure of the eroded thickness and compares relative layer thicknesses for different samples. In such an interpretation, the 45 min anodization forms a thicker oxide than the 25 min anodization. Not only the oxide (part I) but also the transition zone (part II) seems to be thicker which may indicate a difference in the barrier layer thickness between the two samples. The increase of the total oxide thickness for 45 min anodized samples compared with 25 min anodized is also coherent with the Foucault current measured during sample production control (see Section 2.1).

3.4. Electrochemical Behavior of the Anodized Layer

The open circuit potential of 25 min anodized samples was about -415 ± 10 mV vs. Ag/AgCl and about -540 ± 60 mV vs. Ag/AgCl for the 45 min anodized sample. After 75 h of immersion, the potential tended to the values of -430 mV vs. Ag/AgCl for 25 min anodized samples and between -465 and -500 mV vs. Ag/AgCl for the 45 min anodized samples. This indicates a stronger surface evolution during immersion and a slight passivation for the sample anodized with the longer time.

EIS measurements were conducted to describe the evolution of the oxide properties. Examples of Nyquist plots of 25 min and 45 min anodized samples of 2024 (named as 2024–25 min and 2024–45 min), obtained after 2 h, 25 h, 50 h and 75 h of immersion in 0.01 M NaCl aqueous solution, are displayed in Figure 6.

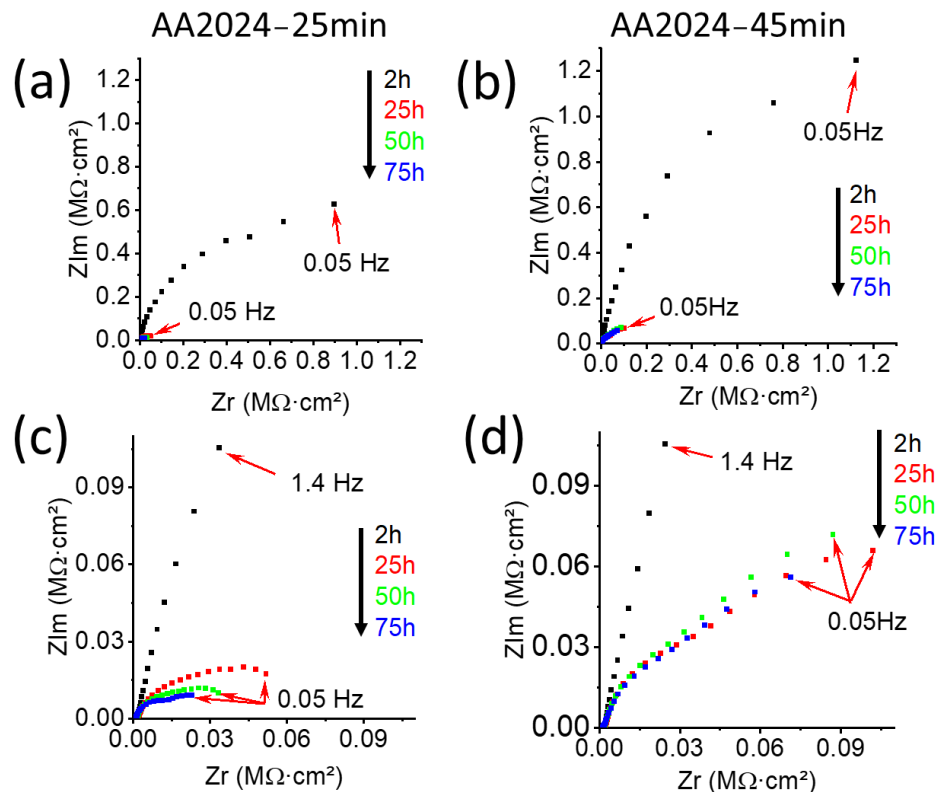


Figure 6. Nyquist plots of 2024 anodized in TSA for 25 min (a,b) and 45 min (c,d), obtained after 2 h (■), 25 h (■), 50 h (■) and 75 h (■) of immersion in 0.01 M NaCl.

For both samples presented in the figure, a flattened semi-circle can be seen on the Nyquist plot recorded after 2 h of immersion with a higher impedance for the 2024–45 min. The impedance of the 2024–45 min sample stays higher than that of 2024–25 min for all immersion times and the difference between them increases during immersion. Higher corrosion resistance is therefore expected for the material anodized for 45 min than for 25 min. A slight white deposit and small black pits were indeed observed on the surface after 75 h of immersion for 25 min of anodizing; no major differences were reported in the case of 45 min anodizing. Images of these surfaces after 75 h of immersion in 0.01 M NaCl can be found in Supplementary Information, Figure S2.

The corresponding Bode diagrams are displayed in Figure 7 after the correction for the electrolyte resistance (its contribution was removed from the plots). The tendencies look similar for the curves representing both samples. After 2 h of immersion, both samples exhibit one contribution at low frequency, attributed for such systems to the barrier layer. Starting from 25 h and up to 75 h of immersion, a new contribution appears at mid/high frequency (around 100 Hz) which is attributed to the oxide layer [9,10,31–33]. For the sample anodized for 25 min, the modulus at 0.05 Hz decreases from 53 $k\Omega \cdot cm^2$ after 25 h up to 24 $k\Omega \cdot cm^2$ after 75 h, while the 45 min anodized sample is more stable in immersion, going from 120 $k\Omega \cdot cm^2$ after 25 h to 89.6 $k\Omega \cdot cm^2$ after 75 h. The modulus drop between 25 h and 75 h is similar for both samples, around 30 $k\Omega \cdot cm^2$, but at equivalent immersion time the modulus value is always higher for the 45 min anodized sample, showing its better immersion stability and better corrosion resistance.

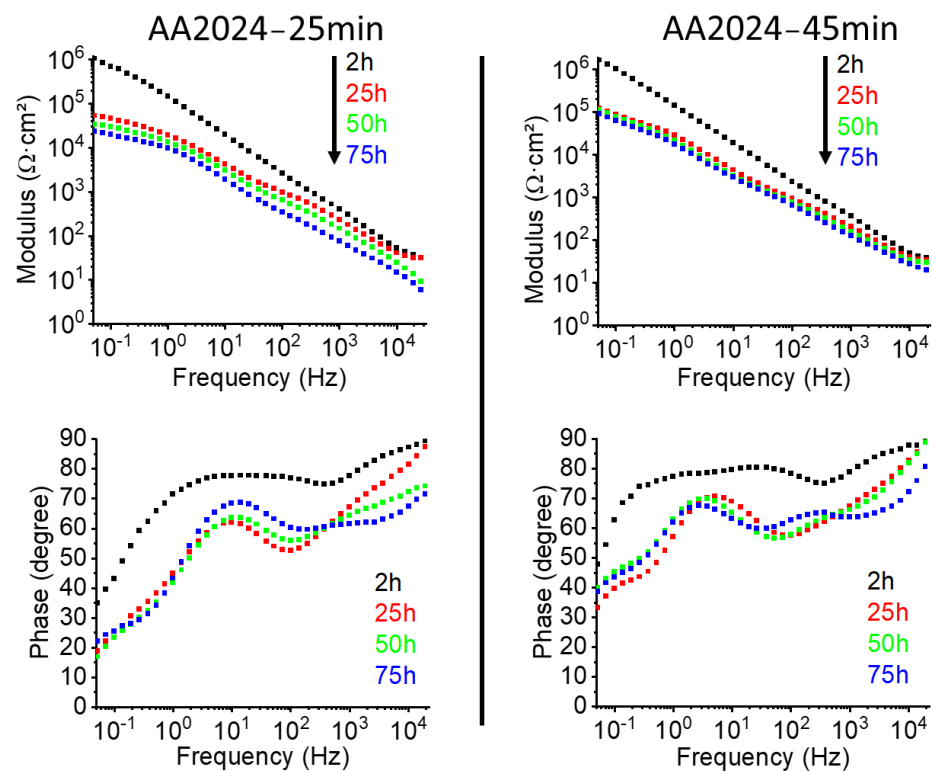


Figure 7. Corrected Bode diagrams of 2024 anodized in TSA for 25 min and 45 min, obtained after 2 h (●), 25 h (●), 50 h (●) and 75 h (●) of immersion in 0.01 M NaCl.

Equivalent Circuit were used to go further into the interpretation of the impedance data. The general model used in the literature for anodic layer is represented in Figure 8a [4,10,31]. R_e corresponds to the electrolyte resistance; $R_{e'}$ is the resistance of the solution inside the pores; R_{pw} is the resistance of the pore walls, and C_{pw} is the associated capacitance. As the porous wall resistivity is high and prevents the current transport, the RC couple R_{pw}/C_{pw} can be neglected. Because of the unsealed pores, the $R_{e'}$ value is very low so the model can be simplified to the schema presented in Figure 8b.

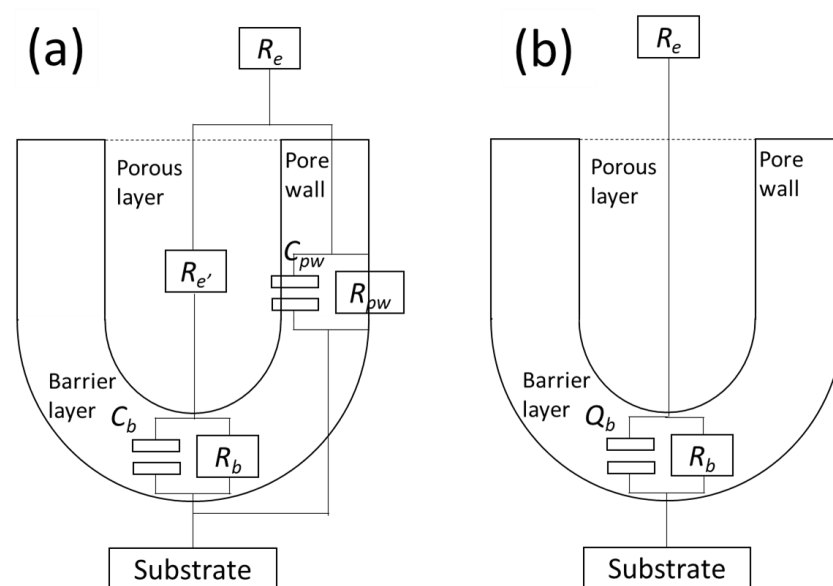


Figure 8. Equivalent circuit proposed for the anodized sample after 2 h of immersion in the 0.01 M NaCl, general model (a) and simplified model (b).

To express the non-ideality of the system, constant phase elements (CPE) are used instead of pure capacitors. Thus, Q_b represents the CPE parameters for the barrier layer and α_b the coefficient that translates this non-ideality (if $\alpha = 1$, the CPE is a pure capacitance while if $\alpha = 0$ the CPE is a pure resistance). In the initial state, after 2 h of immersion, the best fit was obtained with the simplified model of Figure 8b, inspired by the one proposed in [6,13,34,35]. The fitted data are presented in Figure 9; this time the electrolyte resistance was not subtracted from the Bode plots. Fitted parameters values are displayed in Table 4.

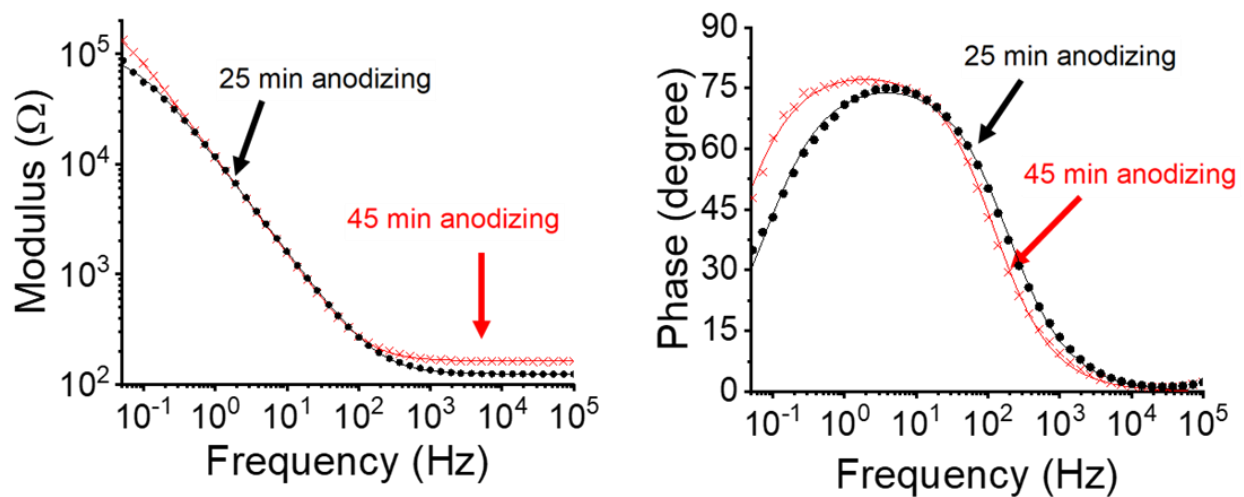


Figure 9. Bode diagrams of the 2024–25 min (●) and 2024–45 min (X), obtained after 2 h of immersion in 0.01 M NaCl. Solid lines represent the fitting curves.

Table 4. Fitted parameter values for the 2024–25 min and 2024–45 min after 2 h of immersion in 0.01 M NaCl.

Parameter	AA2024–25 min			AA2024–45 min	
	Value	Error		Value	Error
R_e (Ω)	123.8	± 0.82		162.7	± 1.0
R_b (Ω)	104.9×10^3	$\pm 2.33 \times 10^3$		259.8×10^3	$\pm 10.1 \times 10^3$
Q_b (S^*s^α)	17.8×10^{-6}	$\pm 0.18 \times 10^{-6}$		16.71×10^{-6}	$\pm 0.15 \times 10^{-6}$
α_b	0.86	$\pm 2.39 \times 10^{-3}$		0.88	$\pm 2.36 \times 10^{-3}$
Goodness of fit	9.67×10^{-4}	/		5.36×10^{-4}	/

As expected, the value of R_e is low and similar for the samples. The parameter α_b for 2024–25 min and 2024–45 min is, respectively, 0.86 and 0.88. The main difference resides in the barrier layer resistance R_b . The R_b of the 2024–45 min sample is almost twice as high as that of the 2024–25 min, demonstrating its stronger corrosion resistance. The equivalent circuit data are in accordance with the results obtained by EIS from the Bode plots.

Expected from EIS higher corrosion resistance of 45 min anodized versus 25 min anodized samples is consistent with the surface state of the samples after 500 h of salt spray tests (SST) (see example of surface appearance in Supplementary Information, Figure S3). After SST, no pits or one pit maximum was detected on 45 min anodized samples while for 25 min anodized samples the results were less reproducible, and in some cases more than 2 pits were found.

To sum up, the electrochemical results seem to support higher immersion stability of the samples anodized for 45 min despite their higher porosity, observed by SEM and GD-OES. Higher R_b values of the 2024–45 min sample compared with the 2024–25 min are coherent with the idea that not only the thickness of the porous but also the barrier layer increases with anodizing time.

4. Discussion

The results presented in this study point out several effects of the anodizing time on the oxide layer properties. First of all, the density of pores is higher for the 45 min anodized than for the 25 min anodized sample (30.0% for 45 min vs. 15.0% for 25 min). Our hypothesis is that as the oxide is in contact with the TSA electrolyte for a longer time, higher porosity can be developed. There are not so many articles on this subject, but one similar idea can be found in the work by Aerts et al. [36]. In theory, such a difference in the porosity can have an impact on the initial adhesion properties of the material. In the aerospace industry, the anodizing step is usually not the last surface treatment to be performed: an organic coating may be applied on the anodized surface to enhance corrosion protection and provide the desired aesthetic aspect of the final product [37]. Thus, the oxide layer is crucial for good paint adherence. Several theories have been proposed to describe how adhesion works, and it is highly probable that this phenomenon occurs through a combination of several mechanisms. Among them, the mechanical interlocking [14] and the adhesion through hydrogen/covalent bonding [3] seem the most appropriate. On a macroscopic level, when the paint penetrates and fills the pores of the anodized surface, mechanical interlocking occurs between the paint and the pores surface. As the porosity of the 45 min-anodized sample is higher than the 25 min-anodized sample, the surface contact area for paint penetration is higher [14]. Thus, a longer anodizing time could be expected to provide better initial adhesion properties through the increased porosity of its anodic layer surface. Moreover, contact angle measurements are in accordance with the microstructure observed through SEM and support this idea: the better wettability of the sample with the longer anodizing cycle should contribute to better initial adhesion properties with subsequent water-based post-treatments (sealing or water-borne paint for example).

Then, both GD-OES and EIS help to understand the role of an increased anodizing time on the immersion stability properties of the oxide layer. GD-OES revealed a thicker oxide layer while EIS highlights that the barrier effect in corrosion resistance is mainly due to the thin (barrier) layer and not to the total thickness of the porous layer. The value of R_b is almost two times higher for the 45 min anodized sample indicating a possible difference in the structure or the thickness of the barrier layer. This is coherent with the increased erosion time of the transition zone of the 45 min anodized sample observed on the GD-OES profile (part II in Figure 5).

According to the literature, higher porosity of 45 min anodized sample can also lead to a lower thermal conductivity if compared with 25 min anodizing [38]; however, this statement needs further verification.

To sum up, while an increased porosity seems to be intuitively not beneficial for corrosion resistance, our results demonstrate that the corrosion resistance is not affected by it; moreover, it seems that the properties of the thin barrier layer are improved. Besides, porosity increase can be interesting for the improvement of adhesion.

5. Conclusions

The effect of the anodizing time on the microstructure and the immersion stability of the TSA anodized aluminum alloy with two different anodizing times (25 and 45 min) was evaluated with SEM, GD-OES and EIS.

- SEM surface observations revealed that increasing anodizing time led to a higher density of pores (30% porosity after 45 min in comparison with 15% after 25 min) which is expected to provide better wettability for aqueous post treatments. This was also supported by contact angle measurement). Higher porosity could also improve initial adhesion of organic coatings via mechanical interlocking mechanism.
- Elemental oxide layer composition seems to be similar between the samples anodized for two different times, but the oxide layer is slightly thicker, and the interface erosion is slower for the 45 min anodized sample. EIS measurements confirm the better corrosion resistance and immersion stability of this sample if compared to 25 min anodized.

- Interpretation of the EIS data allows the attribution of this improvement not to the increase of the thickness of the porous layer but to the improvement of the barrier layer which could be due to its densification or its thickness increase.

Supplementary Materials: The following supporting information can be downloaded at: <https://www.mdpi.com/article/10.3390/met13050993/s1>, Figure S1: Data of pore area from ImageJ (25 min anodizing and 45 min anodizing); Figure S2: Surface appearance of anodized samples for 25 min and 45 min anodizing before immersion (upper images) and after 75 h of immersion in 0.01 M NaCl (lower images); Figure S3: Salt spray test results after 500 h of exposure.

Author Contributions: Conceptualization, P.V.; methodology, P.V. and F.R.; validation, P.V., F.R. and J.E.; investigation, F.R.; resources, J.E.; writing—original draft preparation, F.R. and P.V.; writing—review and editing, F.R., P.V. and J.E.; visualization, F.R.; supervision, P.V.; project administration, P.V. All authors have read and agreed to the published version of the manuscript.

Funding: This research received no external funding.

Data Availability Statement: The data presented in this study are available on request from the corresponding author.

Conflicts of Interest: The authors declare no conflict of interest.

References

1. Vargel, C. *Corrosion of Aluminium*, 2nd ed.; Elsevier: Amsterdam, The Netherlands, 2020; ISBN 978-0-08-099925-8.
2. Peltier, F.; Thierry, D. Review of Cr-Free Coatings for the Corrosion Protection of Aluminum Aerospace Alloys. *Coatings* **2022**, *12*, 518. [[CrossRef](#)]
3. Paz Martínez-Viademonte, M.; Abrahami, S.T.; Hack, T.; Burchardt, M.; Terryn, H. A Review on Anodizing of Aerospace Aluminum Alloys for Corrosion Protection. *Coatings* **2020**, *10*, 30. [[CrossRef](#)]
4. Boisier, G.; Pébère, N.; Druez, C.; Villatte, M.; Suel, S. FESEM and EIS Study of Sealed AA2024 T3 Anodized in Sulfuric Acid Electrolytes: Influence of Tartaric Acid. *J. Electrochem. Soc.* **2008**, *155*, C521. [[CrossRef](#)]
5. Curioni, M.; Skeldon, P.; Koroleva, E.; Thompson, G.E.; Ferguson, J. Role of Tartaric Acid on the Anodizing and Corrosion Behavior of AA 2024 T3 Aluminum Alloy. *J. Electrochem. Soc.* **2009**, *156*, C147. [[CrossRef](#)]
6. García-Rubio, M.; de Lara, M.P.; Ocón, P.; Diekhoff, S.; Beneke, M.; Lavía, A.; García, I. Effect of Posttreatment on the Corrosion Behaviour of Tartaric–Sulphuric Anodic Films. *Electrochim. Acta* **2009**, *54*, 4789–4800. [[CrossRef](#)]
7. Iglesias-Rubianes, L.; Garcia-Vergara, S.J.; Skeldon, P.; Thompson, G.E.; Ferguson, J.; Beneke, M. Cyclic Oxidation Processes during Anodizing of Al–Cu Alloys. *Electrochim. Acta* **2007**, *52*, 7148–7157. [[CrossRef](#)]
8. Kuznetsov, B.; Serdechnova, M.; Tedim, J.; Sarykevich, M.; Kallip, S.; Oliveira, M.P.; Hack, T.; Nixon, S.; Ferreira, M.G.S.; Zheludkevich, M.L. Sealing of Tartaric Sulfuric (TSA) Anodized AA2024 with Nanostructured LDH Layers. *RSC Adv.* **2016**, *6*, 12. [[CrossRef](#)]
9. Marzocchi, V.; Iglesias-Rubianes, L.; Thompson, G.E.; Bellucci, F. The Influence of Tartaric Acid Additions on the Anodizing Behaviour of AA2024-T3 Alloy in Sulphuric Acid. *Corros. Rev.* **2007**, *25*, 461–474. [[CrossRef](#)]
10. González-Rovira, L.; González-Souto, L.; Astola, P.J.; Bravo-Benítez, C.; Botana, F.J. Assessment of the Corrosion Resistance of Self-Ordered Anodic Aluminum Oxide (AAO) Obtained in Tartaric-Sulfuric Acid (TSA). *Surf. Coat. Technol.* **2020**, *399*, 126131. [[CrossRef](#)]
11. Prada Ramirez, O.M.; Tunes, M.A.; Mennucci, M.M.; Sarykevich, M.; Neves, C.; Ferreira, M.G.S.; Pogatscher, S.; De Melo, H.G. Ce Post-Treatment for Increased Corrosion Resistance of AA2024-T3 Anodized in Tartaric-Sulfuric Acid. *Corros. Sci.* **2022**, *204*, 110371. [[CrossRef](#)]
12. Usman, B.J.; Curioni, M. Influence of Temperature on the Corrosion Testing of Anodized Aerospace Alloys. *Corros. Sci.* **2021**, *192*, 109772. [[CrossRef](#)]
13. García-Rubio, M.; Ocón, P.; Curioni, M.; Thompson, G.E.; Skeldon, P.; Lavía, A.; García, I. Degradation of the Corrosion Resistance of Anodic Oxide Films through Immersion in the Anodising Electrolyte. *Corros. Sci.* **2010**, *52*, 2219–2227. [[CrossRef](#)]
14. Abrahami, S.T.; de Kok, J.M.M.; Gudla, V.C.; Ambat, R.; Terryn, H.; Mol, J.M.C. Interface Strength and Degradation of Adhesively Bonded Porous Aluminum Oxides. *Npj Mater. Degrad.* **2017**, *1*, 8. [[CrossRef](#)]
15. Setianto, M.H.; Korda, A.A. Characterization of Tartaric-Sulphuric Acid Anodized 2024-T3 Aluminium Alloys with Anodizing Potential Variation. *J. Phys. Conf. Ser.* **2019**, *1204*, 8. [[CrossRef](#)]
16. Schneider, M.; Kremmer, K. The Effect of Bath Aging on the Microstructure of Anodic Oxide Layers on AA1050. *Surf. Coat. Technol.* **2014**, *246*, 64–70. [[CrossRef](#)]
17. Paz Martínez-Viademonte, M.; Abrahami, S.T.; Havigh, M.D.; Marcoen, K.; Hack, T.; Burchardt, M.; Terryn, H. The Role of Anodising Parameters in the Performance of Bare and Coated Aerospace Anodic Oxide Films. *Coatings* **2022**, *12*, 908. [[CrossRef](#)]

18. Paz Martinez-Viademonte, M.; Abrahami, S.T.; Hack, T.; Burchardt, M.; Terryn, H. Adhesion Properties of Tartaric Sulfuric Acid Anodic Films Assessed by a Fast and Quantitative Peel Tape Adhesion Test. *Int. J. Adhes. Adhes.* **2022**, *116*, 103156. [[CrossRef](#)]
19. Schneider, M.; Gierth, U.; Kremmer, K. An FT-IRRAS-Study of Anodic Oxide Films on Aluminum Alloys and the Impact of Bath Aging. *Appl. Surf. Sci.* **2020**, *522*, 146438. [[CrossRef](#)]
20. Mubarak, M.Z.; Wahab; Sutarno; Wahyudi, S. Effects of Anodizing Parameters in Tartaric-Sulphuric Acid on Coating Thickness and Corrosion Resistance of Al 2024 T3 Alloy. *JMMCE* **2015**, *3*, 154–163. [[CrossRef](#)]
21. García-Rubio, M. Optimisation of a Non-Chromium-Containing TSA Anodising Bath for Aluminium Alloys for Aerospace Industry Application. Ph.D. Thesis, Universidad Autonoma de Madrid, Madrid, Spain, 2009.
22. Saenz de Miera, M.; Curioni, M.; Skeldon, P.; Thompson, G.E. The Behaviour of Second Phase Particles during Anodizing of Aluminium Alloys. *Corros. Sci.* **2010**, *52*, 2489–2497. [[CrossRef](#)]
23. Saenz de Miera, M.; Curioni, M.; Skeldon, P.; Thompson, G.E. Preferential Anodic Oxidation of Second-Phase Constituents during Anodising of AA2024-T3 and AA7075-T6 Alloys. *Surf. Interface Anal.* **2010**, *42*, 241–246. [[CrossRef](#)]
24. Curioni, M.; Saenz de Miera, M.; Skeldon, P.; Thompson, G.E.; Ferguson, J. Macroscopic and Local Filming Behavior of AA2024 T3 Aluminum Alloy during Anodizing in Sulfuric Acid Electrolyte. *J. Electrochem. Soc.* **2008**, *155*, C387. [[CrossRef](#)]
25. Renaud, A.; Poorteman, M.; Escobar, J.; Dumas, L.; Paint, Y.; Bonnaud, L.; Dubois, P.; Olivier, M.-G. A New Corrosion Protection Approach for Aeronautical Applications Combining a Phenol-ParaPhenyleneDiAmine Benzoxazine Resin Applied on Sulfo-Tartaric Anodized Aluminum. *Prog. Org. Coat.* **2017**, *112*, 9. [[CrossRef](#)]
26. Lebouil, S.; Tardelli, J.; Rocca, E.; Volovitch, P.; Ogle, K. Dealloying of Al₂Cu, Al₇Cu₂Fe, and Al₂CuMg Intermetallic Phases to Form Nanoparticulate Copper Films. *Mater. Corros.* **2014**, *65*, 416–424. [[CrossRef](#)]
27. Ding, Z.; Smith, B.A.; Hebert, R.R.; Zhang, W.; Jaworowski, M.R. Morphology Perspective on Chromic Acid Anodizing Replacement by Thin Film Sulfuric Acid Anodizing. *Surf. Coat. Technol.* **2018**, *350*, 31–39. [[CrossRef](#)]
28. Ostapiuk, M.; Bienias, J. Fracture Analysis and Shear Strength of Aluminum/CFRP and GFRP Adhesive Joint in Fiber Metal Laminates. *Materials* **2020**, *13*, 7. [[CrossRef](#)]
29. García-Rubio, M.; Ocón, P.; Climent-Font, A.; Smith, R.W.; Curioni, M.; Thompson, G.E.; Skeldon, P.; Lavía, A.; García, I. Influence of Molybdate Species on the Tartaric Acid/Sulphuric Acid Anodic Films Grown on AA2024 T3 Aerospace Alloy. *Corros. Sci.* **2009**, *51*, 2034–2042. [[CrossRef](#)]
30. Prada Ramirez, O.M.; Queiroz, F.M.; Tunes, M.A.; Antunes, R.A.; Rodrigues, C.L.; Lanzutti, A.; Pogatscher, S.; Olivier, M.-G.; De Melo, H.G. Tartaric-Sulphuric Acid Anodized Clad AA2024-T3 Post-Treated in Ce-Containing Solutions at Different Temperatures: Corrosion Behaviour and Ce Ions Distribution. *Appl. Surf. Sci.* **2020**, *534*, 147634. [[CrossRef](#)]
31. Gonzalez, J.A.; Lopez, V.; Bautista, A.; Otero, E. Characterization of Porous Aluminium Oxide Films from a.c. Impedance Measurements. *J. Appl. Electrochem.* **1999**, *29*, 10.
32. Hoar, T.P.; Wood, G.C. The Sealing of Porous Anodic Oxide Films on Aluminium. *Electrochim. Acta* **1962**, *7*, 333–353. [[CrossRef](#)]
33. Hitzig, J.; Jüttner, K.; Lorenz, W.J.; Paatsch, W. AC-Impedance Measurements on Porous Aluminium Oxide Films. *Corros. Sci.* **1984**, *24*, 945–952. [[CrossRef](#)]
34. Zhao, X.; Zuo, Y.; Zhao, J.; Xiong, J.; Tang, Y. A Study on the Self-Sealing Process of Anodic Films on Aluminum by EIS. *Surf. Coat. Technol.* **2006**, *200*, 6846–6853. [[CrossRef](#)]
35. Fedel, M.; Franch, J.; Rossi, S. Effect of Thickness and Sealing Treatments on the Corrosion Protection Properties of Anodic Oxide Coatings on AA5005. *Surf. Coat. Technol.* **2021**, *408*, 126761. [[CrossRef](#)]
36. Aerts, T.; Dimogerontakis, T.; De Graeve, I.; Franssaer, J.; Terryn, H. Influence of the Anodizing Temperature on the Porosity and the Mechanical Properties of the Porous Anodic Oxide Film. *Surf. Coat. Technol.* **2007**, *201*, 7310–7317. [[CrossRef](#)]
37. Zhang, T.; Zhang, T.; He, Y.; Wang, Y.; Bi, Y. Corrosion and Aging of Organic Aviation Coatings: A Review. *Chin. J. Aeronaut.* **2023**, *36*, 1–35. [[CrossRef](#)]
38. Lee, J.; Kim, Y.; Jung, U.; Chung, W. Thermal Conductivity of Anodized Aluminum Oxide Layer: The Effect of Electrolyte and Temperature. *Mater. Chem. Phys.* **2013**, *141*, 680–685. [[CrossRef](#)]

Disclaimer/Publisher's Note: The statements, opinions and data contained in all publications are solely those of the individual author(s) and contributor(s) and not of MDPI and/or the editor(s). MDPI and/or the editor(s) disclaim responsibility for any injury to people or property resulting from any ideas, methods, instructions or products referred to in the content.